Korean J. Chem. Eng., 34(1), 160-169 (2017)
DOI: 10.1007/s11814-016-0258-4

pISSN: 0256-1115
eISSN: 1975-7220

Porous polyethersulfone hollow fiber membrane in CO_2 separation process via membrane contactor - The effect of nonsolvent additives

Gholamreza Bakeri*,†, Masoud Rezaei-DashtArzhandi, Ahmad Fauzi Ismail**,†, Takeshi Matsuura***, Mohd Sohaimi Abdullah**, and Ng Be Cheer****

*Advanced Membrane and Biotechnology Research Center, Babol Noshirvani University of Technology, Babol, Iran
**Advanced Membrane Technology Research Centre (AMTEC), Universiti Teknologi Malaysia, 81310 Skudai, Johor, Malaysia
***Department of Chemical and Biological Engineering, University of Ottawa, Ottawa, Ontario, Canada K1N 6N5
(*Received 2 April 2016 • accepted 9 September 2016*)

Abstract−A membrane contactor (MC) is used for natural gas sweetening and wastewater treatment with a membrane that is acting as a separating barrier between two phases, usually liquid and gas. The performance of membrane is governed by parameters such as pore size, porosity, tortuosity and surface hydrophobicity, which can be controlled by a number of methods. Addition of nonsolvents to spinning solution is known to be one of such methods. In this study, the effects of low molecular weight additives as phase inversion promoters on the morphology of polyethersulfone hollow fiber membranes and their performance in gas-liquid MC processes were investigated. It was found that among the six nonsolvent additives under study, addition of water resulted in the highest CO_2 flux, by decreasing the thermodynamic stability of polymer solution and maintaining high solvent-nonsolvent exchange rate.

Keywords: Polyethersulfone, Membrane Contactor, Phase Inversion Promoter, Hollow Fiber Membrane

INTRODUCTION

Global warming is a major concern due to its negative effects on human life, such as scarce rainfall, flooding, and drought. Industrial development accelerates this phenomenon as a result of the emission of greenhouse gases into the atmosphere. Therefore, finding solutions for this problem is imperative.

Separation of CO_2, which is known as the major source of global warming, from flue gases and its conversion to less hazardous materials is one of the best ways to overcome this problem. For example, CO_2 can be used in production of biofuel, chemical or petrochemical products such as urea and sodium bicarbonate/carbonate or it can be sent to deep layers of earth or seas to be consumed naturally.

Different methods have been proposed for CO_2 removal, such as absorption, adsorption, and refrigeration, among which absorption is the most popular industrial process. In this process, an absorbent, which can be as cheap as water, is used to remove CO_2 from the gas stream. The absorption process is usually carried out in packed or tray towers, in which operational problems are often faced, such as dependency of liquid and gas flow rates, foaming, flooding, and low contact area.

The membrane contactor is a promising candidate to overcome these difficulties by separating the gas and liquid phases by means of a porous membrane; the solute gas diffuses through the bulk of the gas to the entrance of membrane pores, and then diffuses through the gas-filled pores of the membrane to the other end of the pores to be absorbed by the liquid. The porous membrane provides high contact area between gas and liquid phases and improves the mass transfer rate, e.g., compared to traditional equipment the mass transfer rate increases as much as five times [1].

It is known that the membrane characteristics, such as membrane material, pore size, and porosity, can affect the membrane performance in contactor applications. The pores of the membrane should be gas filled and the penetration of liquid into the membrane pores has to be minimized. For this purpose, membranes for contactor applications are usually made from a limited number of very hydrophobic polymers [2,3] such as polyethylene (PE), polypropylene (PP) and polytetrafluoroethylene (PTFE). Unfortunately, these polymers are not soluble in common solvents and difficult to process. We reported earlier that it is possible to use slightly more hydrophilic material such as polyetherimide (PEI) or polyethersulfone (PES) if the pore size is adjusted correctly, and a slightly higher pressure is applied at the liquid side than at the gas phase [4].

Polyethersulfone (PES) is a polymer with good thermal and chemical stability and has been used widely for membrane fabrication to be used in ultrafiltration process, blood purification, gas separation process etc. Different fabrication conditions have been investigated to change the structure of membrane. Among others, the concentration of polymer plays a critical role in governing the properties of the membrane and, as reported in our earlier publication, the membrane fabricated from 15 wt% PES solution exhibited suitable characteristics to be used in contactor applications [5].

Blending phase inversion promoters have been widely used to alter the structure of membrane. It has a dual effect on the polymer solution; one is that they decrease the thermodynamic stability, which promotes the phase inversion process, and the other is that they increase the viscosity of polymer solution, which reduces

†To whom correspondence should be addressed.
E-mail: bakeri@nit.ac.ir, afauzi@utm.my, ghr_bakeri@yahoo.com
Copyright by The Korean Institute of Chemical Engineers.

the phase inversion rate.

Polymeric additives have been used as phase inversion promoter, even though the solution becomes heterogeneous, in most cases, when they are added into PES solution. Low molecular weight polymers such as polyvinylpyrrolidone (PVP) [6-8] and polyethylene glycol (PEG) [9-11] have been reported as pore formers to fabricate ultrafiltration membranes [7,9,10]. Since blending polymeric additives increases the viscosity of polymer solution, the phase inversion process slows down and fingerlike macrovoids may disappear in the membrane structure [12].

Inorganic additives such as TiO_2 [13-15], silver [16-18], SiO_2 [19,20] and Al_2O_3 [21,22] are another category of phase inversion promoters for PES membrane. They are added to enhance the hydrophilicity of the membrane or to give some specific characteristics (such as antibacterial properties) to the membrane.

Low molecular weight compounds can also be used as phase inversion promoter for PES solution. As these compounds are soluble in water they can be washed out during phase inversion process, affecting the porosity and the pore size of the resultant membrane. The effect of various ethanol amines on the structure and performance of PES nanofiltration membranes was studied elsewhere [23]. Water and alcohols (methanol, ethanol and n-propanol) [24] were used to change the structure of PES hollow fiber membrane, spun from 18 wt% solution and used in ultrafiltration process. As the concentration of ethanol increased from 0 to 25 wt%, the structure of the membrane changed from fingerlike to spongelike structure. Ghasem et al. [25] added o-xylene to PES solution to improve the hydrophobicity of the membrane and used the fabricated membrane in gas-liquid contacting process. O-xylene is not soluble in water and increases the solution viscosity. Blending o-xylene reduces the pore size and enhances the contact angle of membrane, hence increases the hydrophobicity.

The objective of this study was to attempt the blending of low molecular weight phase inversion promoters to PES solution (15 wt%) for spinning porous hollow fiber membranes to be used in membrane gas absorption process. To the best of the authors' knowledge, no investigations have been so far made on this topic.

THEORY

In the membrane gas absorption process, there are three mass transfer resistances in series: (1) the gas side mass transfer resistance, which depends on the composition and flow regime of gas, e.g., it can be neglected in case of pure gas or at high gas flow rate; (2) membrane mass transfer resistance that depends on the characteristics of the membrane such as pore size and its distribution, pore tortuosity, and surface hydrophobicity and is independent of gas and liquid flow rates; (3) the liquid side mass transfer resistance that depends on the type and flow rate of liquid absorbent, e.g., in case of strong absorbent or high liquid flow rate, the transfer resistance can be neglected.

The overall mass transfer resistance can be related to these three resistances according to Eq. 1 [26].

$$\frac{1}{K_{OL}} = \frac{1}{k_l} + \frac{Hd_i}{k_m d_{lm}} + \frac{Hd_i}{k_g d_o} \tag{1}$$

where K_{OL} is the overall mass transfer coefficient, k_l is the liquid side mass transfer coefficient, k_g is the gas side mass transfer coefficient, k_m is the membrane mass transfer coefficient, d_i, d_o and d_{lm} are inner diameter, outer diameter and log mean diameter of the hollow fiber membrane, respectively, and H is Henry's constant that is given elsewhere [27]. The overall mass transfer coefficient can further be measured from the experimental data of absorption process in a membrane contactor as shown in Eq. (2).

$$K_{OL} = \frac{Q_L(C_l^{out} - C_l^{in})}{A\Delta C_l^{av}} \tag{2}$$

where Q_L is the liquid absorbent flow rate, C_l is the solute gas (CO_2) concentration in the liquid, A is the contact area which is calculated based on the inner diameter of hollow fiber membrane as liquid flows in the lumen side and ΔC_l^{av} is the logarithmic mean of transmembrane concentration difference of solute gas in terms of liquid which can be calculated by Eq. (3).

$$\Delta C_l^{av} = \frac{(HC_g^{in} - C_l^{in}) - (HC_g^{out} - C_l^{out})}{\ln\left(\frac{HC_g^{in} - C_l^{in}}{HC_g^{out} - C_l^{out}}\right)} \tag{3}$$

The third term on the right side of Eq. (1) can be omitted as the gas used in this study is pure CO_2. The liquid side mass transfer coefficient (k_l) is related to the liquid velocity according to Eq. (4) [28].

$$Sh_L = \sqrt[3]{3.67^3 + 1.62^3 Gz} \tag{4}$$

where Sh is Sherwood number ($k_l d_i/D$), Gz is Graetz number ($V_{liquid} D_i^2/DL$), V_{liquid} is the liquid velocity, D is the diffusivity of solute gas in the liquid and L is the length of hollow fiber.

EXPERIMENTAL

1. Materials

Polyethersulfone (PES) was purchased from Arkema Inc. and was dried at 70 °C overnight before being used for dope preparation. N-methyl-2-pyrrolidione (NMP) [CAS No. 872-50-4] with a purity of 99.5 wt% was purchased from Merck and was used as solvent. Distilled water, methanol with a purity of 99.8 wt% was supplied from Sigma Aldrich, ethanol with a purity of 99.5 wt%, glycerol with a purity of 99.5 wt%, acetic acid with a purity of 99.8 wt% and acetone with a purity of 99.8 wt% were all supplied from Merck. They were used as phase inversion promoters to PES solution without further purification.

2. Preparation of Spinning Solutions

A predetermined amount of PES was dissolved in NMP at 70 °C and under gentle mixing to make 25 wt% PES solution. This polymer solution was further mixed with predetermined amounts of nonsolvent additive and NMP to make the solution with 15 wt% PES and 4 wt% nonsolvent additive, with the ratio of nonsolvent additive/NMP 0.05. A solid phase was formed upon blending of nonsolvent additive, but it was soon re-dissolved with gentle mixing at room temperature. In Table 1, the compositions of spinning solutions are presented.

Considering the nonsolvent additive as a part of the solvent, the solution code is given as follows:

Table 1. The compositions of the polymer solutions

Solution no.	PES (wt%)	Nonsolvent/ NMP	Solvent (wt%)[a]	Type of nonsolvent
#M1	15	0.05	85	Water
#M2	15	0.05	85	Methanol
#M3	15	0.05	85	Ethanol
#M4	15	0.05	85	Glycerol
#M5	15	0.05	85	Acetic acid
#M6	15	0.05	85	Acetone
#M7	15	0	85	-

[a]Nonsolvent additive is considered as a part of the solvent

(NMP+water) for solution #M1; (NMP+methanol) for solution #M2; (NMP+ethanol) for solution #M3; (NMP+glycerol) for solution #M4; (NMP+acetic acid) for solution #M5; (NMP+acetone) for solution #M6.

The membrane code is the same as the code of the solution from which the hollow fiber was spun.

3. Preparation of Hollow Fibers

The hollow fiber fabrication process was described elsewhere in detail [29]. Briefly, the spinning solution was delivered to the annulus of a tube-in-orifice spinneret at constant flow rate while water as the bore fluid was sent to the inner tube of the spinneret. After leaving the spinneret, the nascent fiber passed through the air gap and entered the coagulation bath (tap water) to complete the phase inversion process. The wet spun fibers were immersed in water for three days to remove the residual solvent and nonsolvent additives and then dried naturally by hanging vertically at 20 °C. The spinning conditions are listed in Table 2.

4. Viscosity and Cloud Point Measurement

The viscosity of spinning solution was measured using a viscometer, EW-98965-40, Cole Parmer, USA. For the cloud point measurement, the coagulant (water) was added dropwise from a burette to a predetermined amount of polymer solution under gentle stirring at room temperature until the solution remained cloudy for a few hours. The amount of water needed to reach the cloud point was determined by weighting the solution before and after the addition of the coagulant. Then, the solution composition at the cloud point was calculated.

5. Hollow Fiber Module Preparation and Gas Permeation Test

The gas permeation test [30] was used to measure the mean pore size and the effective surface porosity, which is the ratio of surface porosity to the effective length of the pore. Even though the pore size obtained from gas permeation test does not have physical meaning [31], the results can be used for comparison of fabricated membranes.

Table 2. Spinning conditions for fabrication of the hollow fiber membranes

Bore fluid	Distilled water
External coagulant	Tap water
Air gap (cm)	1
Bore fluid temperature (°C)	20
External coagulant temperature (°C)	20

In this test, it is assumed that the pores are cylindrical and straight and the flow of gas through the pores of membrane is in the Poiseuille and Knudsen flow regimes. Therefore, the total gas permeance through the membrane can be given by Eq. (5).

$$\overline{P} = P_K + P_P = \frac{2}{3}\left(\frac{8RT}{\pi M}\right)^{0.5} \frac{r_{P,m}\,\xi}{RT\,L_P} + \frac{1}{8\mu}\frac{r_{P,m}^2\,\xi}{RT\,L_P}\overline{p} \qquad (5)$$

$$\overline{P} = A + B\overline{p}$$

where $\overline{P}$ is the total gas permeance, P_K is the gas permeance in the Knudsen flow regime, P_P is the gas permeance in the Poiseuille flow regime, R is the universal gas constant, T is absolute temperature, M is molecular weight of gas, $r_{P,m}$ is the mean pore radius, μ is the viscosity of gas, ξ is the surface porosity (A_P/A_T where A_P is area of pores and A_T is total area of membrane), L_P is the effective pore length and $\overline{p}$ is the mean pressure ($p_u+p_d/2$ where p_u is upstream pressure and p_d is downstream pressure). Therefore, the plot of total gas permeance ($\overline{P}$) versus mean pressure ($\overline{p}$) should be a straight line where the slope and intercept are used in Eqs. (6)-(7) to calculate the mean pore size and effective surface porosity (ξ/L_p) of the membrane.

$$r_{P,m} = \frac{16}{3}\frac{B}{A}\left(\frac{8RT}{\pi M}\right)^{0.5}\mu \qquad (6)$$

$$\frac{\xi}{L_P} = \frac{8\pi RTB}{r_{P,m}^2} \qquad (7)$$

6. Measurement of Liquid Entry Pressure of Water (LEPw)

The wettability resistance is very important for the membrane to be used in contactor applications, as pore wetting by the liquid increases the mass transfer resistance rapidly. The wettability resistance depends both on the surface hydrophobicity and the pore size of the membrane according to the Laplace equation (Eq. (8)).

$$\Delta p = \frac{2\sigma\cos\theta}{r_P} \qquad (8)$$

where σ is the surface tension of liquid, θ is the contact angle between liquid and membrane surface and r_p is the pore radius. LEPw is a simple test to measure the wettability resistance where water is sent to the lumen side of the fiber and the pressure of water is increased with a step size of 0.2 bar. At each pressure, the pressure was kept constant for at least 15 minute. The pressure at which the first droplet of water appears on the outer surface of membrane is reported as LEPw.

7. Membrane Porosity and Tortuosity

The membrane porosity depends mostly on the structure of membrane sublayer such as the type and numbers of voids even though the dead-end pores are not effective on the mass transfer process.

The method to measure the membrane porosity was described elsewhere [32]. Briefly, the weight and length of wet and dried membrane are measured and the porosity of membrane (ε) is calculated through Eqs. (9)-(13).

$$F = \frac{\text{dry membrane weight}}{\text{wet membrane weight}} \qquad (9)$$

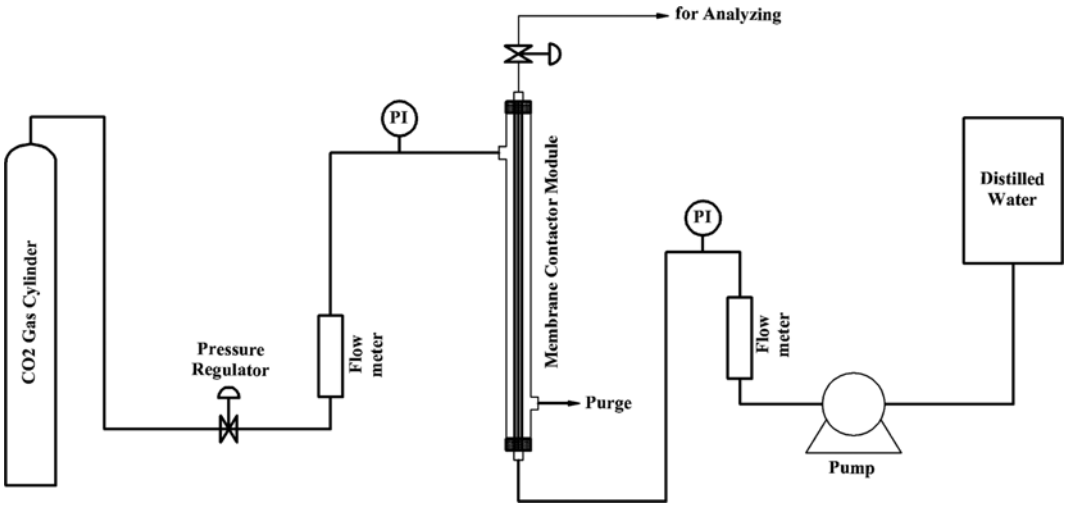

Fig. 1. Schematic of membrane contactor test system.

$$S_l = \frac{\text{wet membrane length} - \text{dry membrane length}}{\text{wet membrane length}} \quad (10)$$

$$E = 1 - (1 - S_l)^3 \quad (11)$$

$$\rho_m = \frac{F}{\left(\frac{F}{\rho_P} + \frac{1-F}{\rho_{water}}\right)(1-E)} \quad (12)$$

$$\varepsilon = \frac{\frac{1}{\rho_m} - \frac{1}{\rho_P}}{\frac{1}{\rho_m}} \quad (13)$$

where F is the mass fraction of polymer in the membrane, S_l is the longitudinal shrinkage of hollow fibers, E is the overall shrinkage of membrane during drying, ρ_m is the density of membrane, ρ_{water} is the water density and ρ_P is the polymer density which is 1.55 g cm^{-3} for PES.

The membrane tortuosity determines the actual diffusion length of solute gas through the membrane and depends on the shape of voids in the membrane sublayer: the more spongelike structure the higher the tortuosity. The tortuosity of membrane (τ) can be calculated by Eq. (14), using the porosity of membrane [33].

$$\tau = \frac{(2-\varepsilon)^2}{\varepsilon} \quad (14)$$

As the tortuosity of fingerlike macrovoids is small, it can be concluded by Eq. (14) that the porosity of the fingerlike structure is high.

8. Scanning Electron Microscopy (SEM)

SEM was used to observe the structure of membrane cross section. The fiber was broken in liquid nitrogen to attain a smooth surface and then platinum (Pt) sputtered. The micrographs were taken by SEM (TM 3000, Hitachi) with a magnification of 150 and 400.

9. Gas Absorption Test

Short-term CO_2 absorption involved using water as absorbent to compare the performance of the fabricated membranes in contactor applications, delivering water in the lumen side and pure CO_2 in the shell side. The pressure of gas and water was 1 and 1.5 bar, respectively, to prevent the gas from bubbling into the liquid. The schematic of the absorption system is shown in Fig. 1 where the liquid flow rate is adjusted by the valve at the exit.

Table 3. The specifications of the contactor module and operating conditions for gas absorption

D_{shell}	1 cm
Effective length of contactor	18 cm
Number of fibers	7
Gas	Pure CO_2
Liquid	Distilled water
P_{gas} (bar)	1 barg
P_{liquid}	1.5 barg
T	298 K
Q_{gas}	1 L/min @ 0 barg

The concentration of CO_2 in the exit liquid was determined by titration method, using 0.5 M NaOH solution as titrant and phenolphthalein solution as the end point indicator. The CO_2 absorption flux is calculated by Eq. (15).

$$\text{Flux} = \frac{Q_L(C_l^{out} - C_l^{in})}{A} \quad (15)$$

The specifications of the contactor module and operating conditions for gas absorption process are presented in Table 3.

RESULTS AND DISCUSSION

1. Morphological Studies

The helium gas permeance versus mean pressure for the fabricated membranes is shown in Fig. 2, where the permeance of all membranes increases with mean pressure, which means Poiseuille flow regime cannot be ignored.

The membrane characterization test results are presented in Table

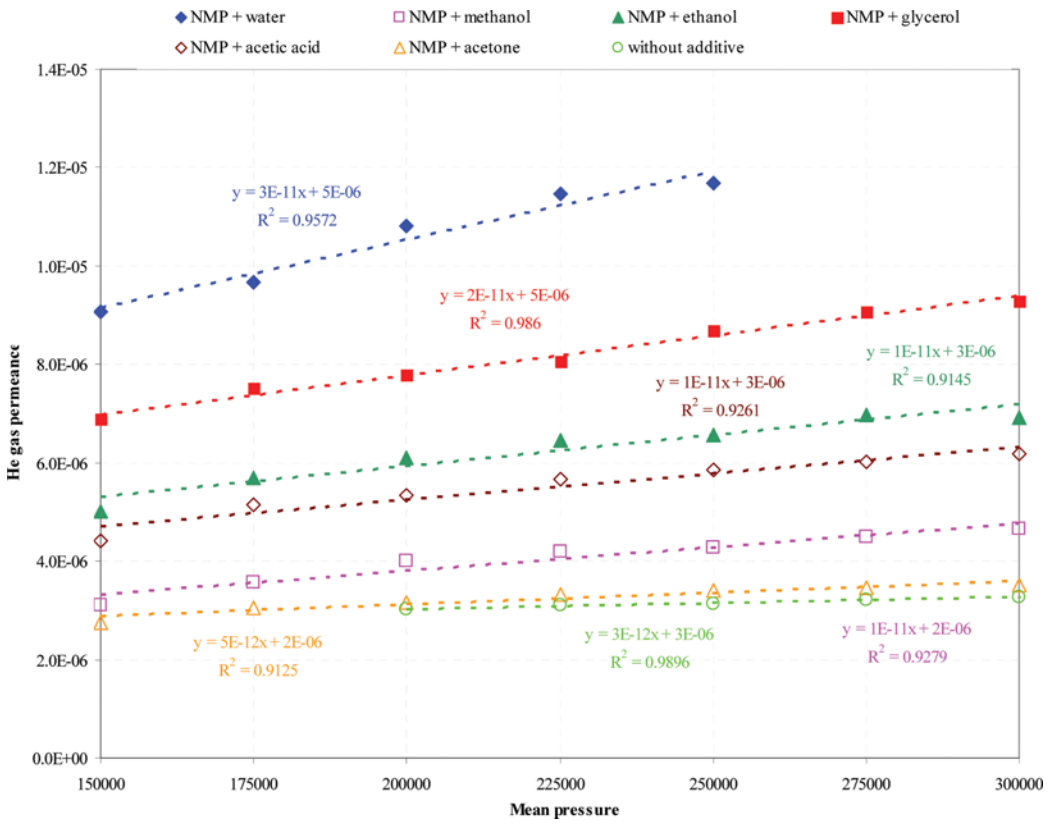

Fig. 2. The plot of helium gas permeance (in terms of mol m^{-2} Pa^{-1} s^{-1}) versus mean pressure (Pa) for the fabricated membranes; (for #M7, data was taken from Chemical Engineering Research and Design 92 (2014) 1381-1390).

4. From the table, membrane #M1 (NMP+water) shows the highest helium gas permeance, resulting in the biggest mean pore size and highest effective surface porosity.

These properties of membrane #M1 can be ascribed to the least stable polymer solution M1. As shown in Table 5, amount of the coagulant (water) which is needed for solution M1 to reach the cloud point is the least. According to the table, the thermodynamic stability of the polymer solutions is in the order of:

Table 4. The characterization tests results for the fabricated membranes

	Membrane number						
	#M1	#M2	#M3	#M4	#M5	#M6	#M7[a]
Mean pore size ($r_{p,m}$) (nm)	653	595	467	630	630	350	163
Standard deviation of $r_{p,m}$	64	50	0	99	99	0	33
Effective surface porosity (ESP) (m^{-1})	28	10	19	22	10	17	55
Standard deviation of ESP	4	1	0	7	1	0	11.2
Gas permeation rate[b] (GPR) @ 1 bar	30386	12138	15539	21893	13191	9257	10291[c]
Standard deviation of GPR	1106	2868	1068	810	1715	377	663.6
Membrane thickness (MT) (mean) (μm)	150.7	139.3	143.7	141.1	147.6	149.5	168.4
Standard deviation of MT	30.5	6.3	26.3	28.9	17.6	30.3	-
LEPw	4.2	3.0	4.2	1.2	4.6	4.4	4.4
Membrane porosity	0.805	0.815	0.841	0.839	0.848	0.842	0.834
Membrane tortuosity	1.77	1.72	1.60	1.61	1.57	1.59	1.63

[a]Data was taken from Chemical Engineering Research and Design 92 (2014) 1381-1390

[b]In terms of $\frac{10^6\ cm^3(STP)}{cm^2\ cmHg\ s}$

[c]It was measured @ 2 bar

Table 5. The viscosity and cloud point test results for spinning solutions

Solution no.	Solution viscosity (cP)	g Water/ 100 g solution	PES (wt%) at cloud point
#M1	216.8	7.5	13.96
#M2	132.7	10.6	13.56
#M3	144.6	10.8	13.54
#M4	228.1	9.6	13.69
#M5	172.3	10.7	13.55
#M6	135.8	11.5	13.46
#M7	180	11.99	13.39

#M1<#M4<#M2<#M5<#M3<#M6

The low thermodynamic stability of polymer solution provides more susceptible regions for penetration of coagulant; therefore, the surface porosity increases. This phenomenon was also observed in our earlier study [34] of polyetherimide hollow fiber membrane. Compared with the cloud point of neat 15 wt% PES solution (11.99 g water/100 g solution) acetone does not have any significant effect on the thermodynamic stability of PES solution.

Furthermore, compared with the viscosity of neat PES solution (180 cp), water (#M1) and glycerol (#M4) enhance the solution viscosity due to their stronger interaction with the solvent and delays the phase inversion process especially in the membrane sublayer.

By dividing the solid contents listed in Table 5 in two groups, a group of (#M5, #M3 and #M6) whose solid contents are lower than the other group of (#M1, #M4 and #M2), and dividing the membrane porosities listed in Table 4 into a group of (#M3, #M6, #M5) whose porosities are higher than those of the other group (#M1, #M2, and #M4), it can be concluded that lower solid contents at the cloud points correspond to higher membrane porosities. As for the tortuosity listed in Table 4, #M1 (NMP+water) has the highest tortuosity that can reduce the absorption flux.

The viscosity of polymer solution strongly affects the mutual exchange rate of solvent and coagulant [35,36]. The slower the solvent-coagulant exchange, the less macrovoids are formed. Both thermodynamic stability and viscosity of polymer solution were reported to affect the membrane structure [37], but it seems that

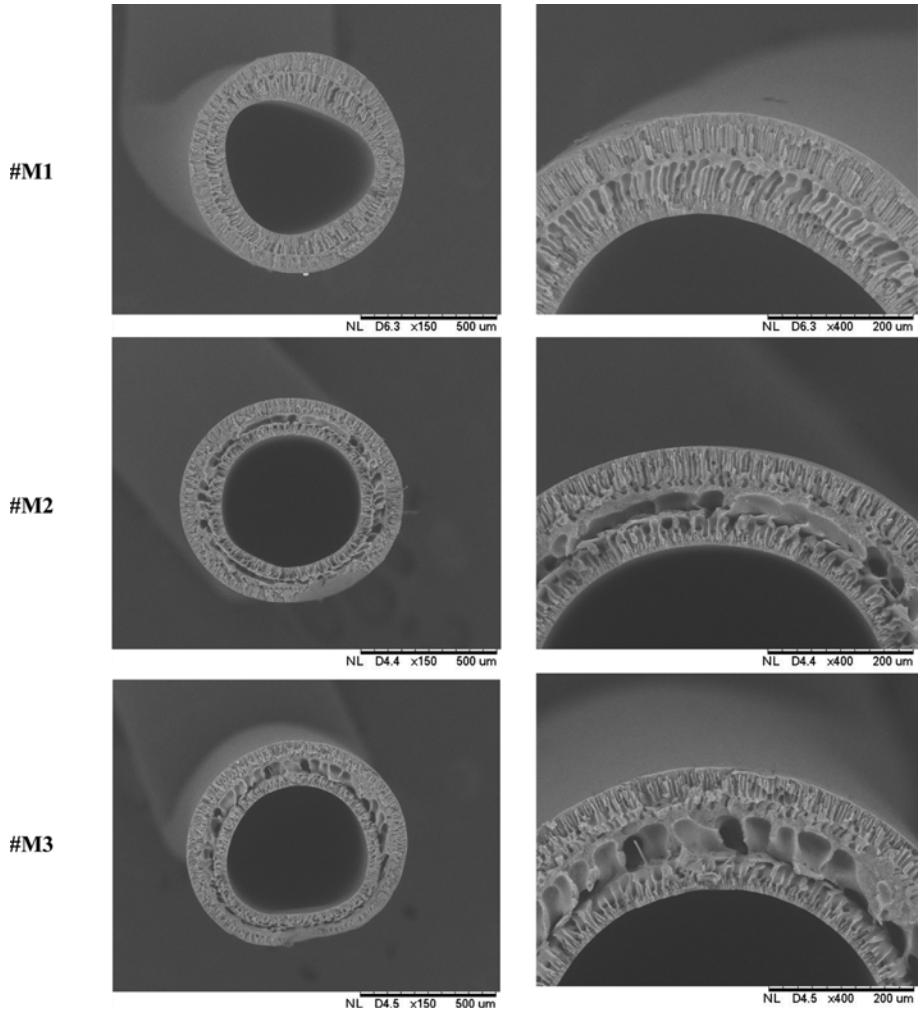

Fig. 3. SEM micrographs for the cross section of the fabricated membranes; (*from Chemical Engineering Research and Design 92 (2014) 1381-1390).

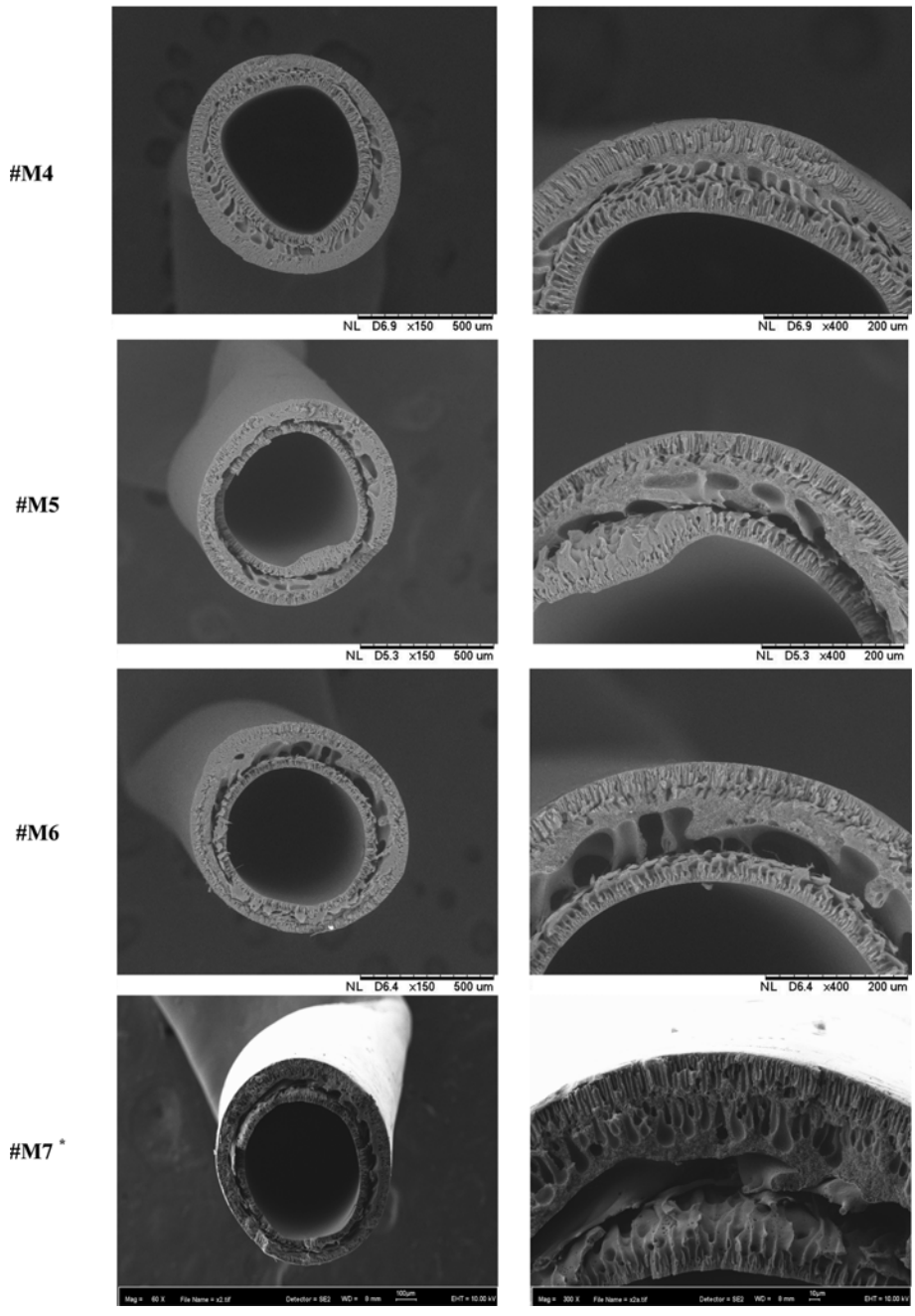

Fig. 3. Continued.

the effect of the latter is more on the membrane sublayer.

The SEM micrographs of the fabricated membranes are shown in Fig. 3, where all the membranes show fingerlike macrovoids originating from the inner and outer surfaces of membrane and extend to the middle of membrane cross-section. It is interesting that from the solutions of lower viscosities (#M3, #M6 and #M2), large macrovoids are formed in the center region of the cross-section. Furthermore, all the membranes show the skin layers on the inner and outer surfaces, caused by the use of strong coagulant (water) both as the internal and external coagulants.

Also, note that the membranes with large macrovoids (#M3, #M6 and #M2) belong to the group of membranes of large porosities (#M3, #M6 and #M5) except for the membrane #M2. Furthermore, the higher the fingerlike macrovoid content in the membrane structure, the less the tortuosity of the membrane. Thus, fingerlike macrovoids decrease the effective path length through the membrane and can be considered as the favorite structure for contactor applications even though big macrovoids may extend to the surface of membrane and reduce the wettability resistance of membrane as was reported elsewhere [38].

2. CO_2 Absorption Tests

The CO_2 absorption flux of the fabricated membranes versus liquid velocity is shown in Fig. 4, where at low liquid velocity, the absorption fluxes of all the membranes are nearly the same due to

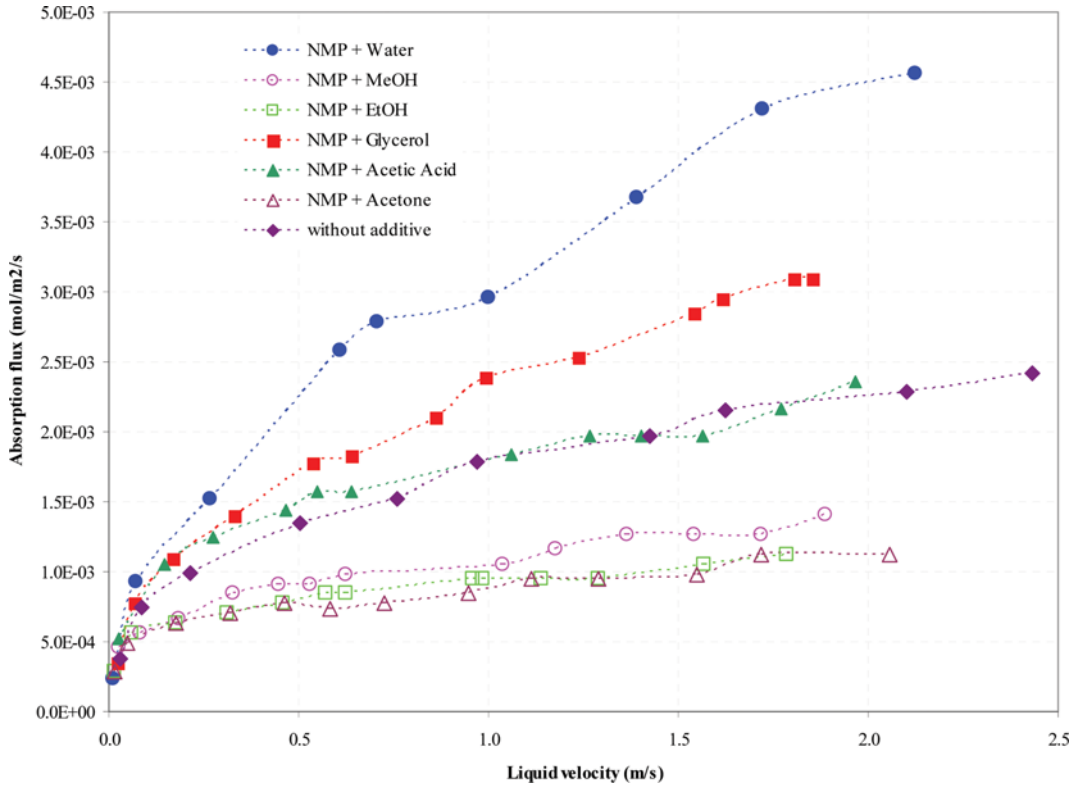

Fig. 4. The plot of average absorption flux of fabricated membranes versus liquid velocity; distilled water in lumen side, pure CO_2 in shell side; (for #M7, data was taken from Chemical Engineering Research and Design 92 (2014) 1381-1390).

the predominance of the liquid side mass transfer resistance in the overall mass transfer resistance. As the liquid velocity increases, the resistance on the liquid side decreases and when the liquid velocity is beyond a limit (V_l), the mass transfer rate depends only on the membrane resistance and is independent of the liquid velocity, i.e., the absorption flux levels off. The lower the membrane mass transfer resistance the higher the V_l.

The membrane pore size affects the membrane mass transfer resistance in two ways: the bigger the pore size, the higher the transfer rate as the mechanism of diffusion through membrane pores shifts to bulk diffusion and the effective diffusivity D_e increases, as shown in Eq. (15) [39].

$$D_e = \frac{1}{\frac{1}{D} + \frac{3}{2r}\sqrt{\frac{\pi M}{8RT}}} \tag{16}$$

On the other hand, the larger pores facilitate the penetration of liquid into pores as shown by the Laplace equation (Eq. (8)), and decrease the transfer rate.

Furthermore, the membrane sublayer has strong effects on the mass transfer as the solute gas should diffuse through the pores of the membrane and the shape of the pores (fingerlike or spongelike) determines the effective diffusion path. In addition, the higher surface porosity has a positive effect on the absorption flux.

The absorption fluxes of fabricated membranes (Fig. 4) show that the membrane #M1 (NMP+water) has the highest flux due to its high surface porosity and fingerlike structure in the membrane sublayer. Note that membrane #M4 (NMP+glycerol) ranks the second in absorption flux. Considering the data in Tables 4-5, the spinning solution #M4 is more thermodynamically stable than #M1 and has lower surface porosity. Despite low porosity and high tortuosity of membrane #M1 and membrane #M4 (Table 4), the absorption flux of these membranes is higher due to the high surface porosity.

It might be interesting to compare the results obtained in this research with those reported earlier [34] for the effect of nonsolvent additives in the PEI spinning dope. In both cases, water was the strongest nonsolvent and the membranes fabricated from the water containing spinning dope had the highest surface porosity. In case of PES membrane, the membrane showed the highest absorption flux, when water was added to the spinning dope, as the sublayer of membrane had finger-like macrovoids. On the other hand, in the case of PEI solution, the membrane did not show the highest absorption flux, as the sublayer had sponge-like structure. The difference is therefore in the sublayer structure of PEI (sponge-like) and PES (finger-like), which was caused by the difference in solution viscosity; i.e., the viscosity of PES solution was lower than that of PEI solution. The results demonstrate the importance of polymer solution viscosity on the performance of membrane that is used in contactor applications and will be investigated more in our forthcoming publication. In summary, in terms of polymer solution properties, the best condition for fabrication of membrane to be used in contactor applications is low thermodynamic stability and low solution viscosity.

Table 6. The mass transfer resistance for the fabricated membranes

Membrane no.	Mass transfer resistance (s/m)
#M1	2569
#M2	42991
#M3	60776
#M4	9606
#M5	17099
#M6	58667
#M7[a]	17285

[a]From Chemical Engineering Research and Design 92 (2014) 1381-1390

To measure the membrane mass transfer resistance, the absorption fluxes of fabricated membranes at high liquid velocity are used, as at high liquid velocity the liquid side transfer resistance can be omitted. Furthermore, since pure CO_2 gas at high volumetric flow rate was used in absorption test, the gas side transfer resistance is negligible and the CO_2 transfer rate depends solely on the membrane resistance.

The CO_2 absorption results in membrane contactor were used to measure the membrane resistance. The overall mass transfer coefficient (K_{OL}) was obtained using Eq. (2) and the liquid side mass transfer coefficient (k_l) was calculated through Eq. (4) using the highest liquid velocity in the plot of average CO_2 absorption flux versus liquid velocity. The membrane mass transfer resistance, $Hd_i/k_m d_{lm}$, (Eq. (1)) was calculated as $(1/K_{OL})-(1/k_l)$ considering that the gas side resistance is negligible as pure gas at high velocity was used. The results were presented in Table 6.

The low mass transfer resistance of membrane #M1 can be related to its large pore size and high LEPw, which provides rapid CO_2 transfer through the membrane pores without significant pore wetting. In addition, the small pore size and low effective surface porosity of membranes #M3 and #M6 increase the mass transfer resistance of these membranes.

CONCLUSIONS

Polyethersulfone hollow fiber membranes were fabricated via dry-wet spinning method, while nonsolvent additives were used to alter the phase inversion process. The fabricated membranes were characterized by different test methods and were applied in CO_2 gas absorption process in a membrane contactor. The conclusions are as follow.

1. The addition of the nonsolvent additives makes the spinning dope more viscous and thermodynamically less stable.

2. Water as nonsolvent additive makes the PES solution less stable than the other nonsolvents, as evidenced by the least amount of coagulant required to reach the cloud point when water is the nonsolvent additive.

3. The fabricated membranes show fingerlike macrovoids in their cross-sectional images, which is related to the low solution viscosity and strong internal and external coagulants.

4. The fabricated membranes show high porosity (more than 80%) and LEPw that are desirable for contactor applications.

5. The membrane fabricated from PES/water/NMP solution shows the highest absorption flux (100% higher than neat membrane), which is related to its highest surface porosity and relatively low membrane tortuosity.

6. The best conditions for the fabrication of membrane to be used in contactor applications in terms of polymer solution are low thermodynamic stability and low solution viscosity.

NOMENCLATURE

A : contact area [m^2]
A_P : area of pores [m^2]
A_T : area of membrane [m^2]
C_l : solute gas concentration in liquid [mol m^{-3}]
ΔC_l^{av} : logarithmic mean of transmembrane concentration difference of solute gas in terms of liquid [mol m^{-3}]
D : bulk diffusivity [m^2 s^{-1}]
D_e : effective diffusivity [m^2 s^{-1}]
d_i : inner diameter of hollow fiber [m]
d_{lm} : log mean diameter of hollow fiber [m]
d_o : outer diameter of hollow fiber [m]
Gz : Graetz number
H : Henry's constant
k_g : gas side mass transfer coefficient [m s^{-1}]
k_L : liquid side mass transfer coefficient [m s^{-1}]
k_m : membrane mass transfer coefficient [m s^{-1}]
K_{OL} : overall mass transfer coefficient [m s^{-1}]
L : length of hollow fiber [m]
L_P : effective pore length [m]
M : molecular weight [Kg mol^{-1}]
P_K : gas permeance under Knudsen flow regime [mol m^{-2} Pa^{-1} s^{-1}]
P_P : gas permeance under Poiseuille flow regime [mol m^{-2} Pa^{-1} s^{-1}]
$\overline{P}$: total gas permeance [mol m^{-2} Pa^{-1} s^{-1}]
$\overline{p}$: mean pressure [Pa]
p_u : upstream pressure [Pa]
p_d : downstream pressure [Pa]
Q_L : liquid flow rate [m^3 s^{-1}]
R : universal gas constant [8.314 J mol^{-1} K^{-1}]
r_p : pore radius [m]
$r_{P,m}$: mean pore radius [m]
V_{liquid} : liquid velocity [m s^{-1}]
Sh : Sherwood number
T : absolute temperature [K]
ξ : surface porosity
σ : surface tension of liquid [N m^{-1}]
ε : membrane porosity
ρ : density [g cm^{-3}]
τ : membrane tortuosity
θ : contact angle between liquid and membrane surface
μ : viscosity [Pa·s]

REFERENCES

1. R. Pogaku and R. H. Sarbatly, *Advances in biofuels*, Springer, New

York (2013).
2. A. Comite, C. Costa, R. Di Felice, P. Pagliai and D. Vitiello, *Korean J. Chem. Eng.*, **32**(2), 239 (2015).
3. D. Jeong, M. Yun, J. Oh, I. Yum and Y. Lee, *Korean J. Chem. Eng.*, **27**(3), 939 (2010).
4. Gh. Bakeri, A. F. Ismail, M. Rahimnejad, T. Matsuura and D. Rana, *Sep. Purif. Technol.*, **98**, 262 (2012).
5. Gh. Bakeri, A. F. Ismail, M. Rahimnejad and T. Matsuura, *Chem. Eng. Res. Des.*, **92**, 1381 (2014).
6. L. Y. Lafreniere, F. D. F. Talbot, T. Matsuura and S. Sourirajan, *Ind. Eng. Chem. Res.*, **26**(11), 2385 (1987).
7. I. M. Wienk, F. H. A. Olde Scholtenhuis, T. van den Boomgaard and C. A. Smolders, *J. Membr. Sci.*, **106**, 233 (1995).
8. B. H. Su, P. Fu, Q. Li, Y. Tao, Z. Li, H. S. Zao and C. S. Zhao, *J. Mater. Sci. Mater. Med.*, **19**, 745 (2008).
9. Y. Liu, G. H. Koops and H. Strathmann, *J. Membr. Sci.*, **223**, 187 (2003).
10. Z. L. Xu and F. A. Qusay, *J. Appl. Polym. Sci.*, **91**, 3398 (2004).
11. B. K. Chaturvedi, A. K. Ghosh, V. Ramachandhran, M. K. Trivedi, M. S. Hanra and B. M. Misra, *Desalination*, **133**, 31 (2001).
12. A. F. Ismail and A. R. Hassan, *Sep. Purif. Technol.*, **55**, 98 (2007).
13. A. Razmjou, A. Resosudarmo, R. L. Holmes, H. Li, J. Mansouri and V. Chen, *Desalination*, **287**, 271 (2012).
14. A. Razmjou, J. Mansouri, V. Chen, M. Lim and R. Amal, *J. Membr. Sci.*, **380**, 98 (2011).
15. A. Sotto, A. Rashed, R. X. Zhang, A. Martínez, L. Braken, P. Luis and B. Van der Bruggen, *Desalination*, **287**, 317 (2012).
16. H. Basri, A. F. Ismail, M. Aziz, K. Nagai, T. Matsuura, M. S. Abdullah and B. C. Ng, *Desalination*, **261**, 264 (2010).
17. H. Basri, A. F. Ismail and M. Aziz, *Desalination*, **273**, 72 (2011).
18. X. Cao, M. Tang, F. Liu, Y. Nie and C. Zhao, *Colloids Surf., B*, **81**, 555 (2010).
19. J. N. Shen, H. M. Ruan, L. G. Wu and C. J. Gao, *Chem. Eng. J.*, **168**, 1272 (2011).
20. A. Ananth, G. Arthanareeswaran and H. Wang, *Desalination*, **287**, 61 (2012).
21. N. Maximous, G. Nakhla, K. Wong and W. Wan, *Sep. Purif. Technol.*, **73**, 294 (2010).
22. L. F. Han, Z. L. Xu, Y. Cao, Y. M. Wei and H. T. Xu, *J. Membr. Sci.*, **372**, 154 (2011).
23. Y. Mansourpanah and A. Gheshlaghi, *J. Polym. Res.*, **19**(13), 1 (2012).
24. Z. L. Xu and F. Alsalhy Qusay, *J. Membr. Sci.*, **233**, 101 (2004).
25. N. Ghasem, M. Al-Marzouqi and L. Zhu, *Sep. Purif. Technol.*, **92**, 1 (2012).
26. A. Gabelman and S. T. Hwang, *J. Membr. Sci.*, **159**, 61 (1999).
27. D. Q. Zheng, T. M. Guo and H. Knapp, *Fluid Phase Equilib.*, **129**, 197 (1997).
28. H. Kreulen, C. A. Smolders, G. F. Versteeg and W. P. M. van Swaaij, *J. Membr. Sci.*, **78**, 197 (1993).
29. M. Rezaei, A. F. Ismail, Gh. Bakeri, S. A. Hashemifard and T. Matsuura, *Chem. Eng. J.*, **260**, 875 (2015).
30. H. H. Park, C. W. Lim, H. D. Jo, W. K. Choi and H. K. Lee, *Korean J. Chem. Eng.*, **24**(4), 693 (2007).
31. A. Mansourizadeh, A. F. Ismail, M. S. Abdullah and B. C. Ng, *J. Membr. Sci.*, **355**, 200 (2010).
32. Gh. Bakeri, A. F. Ismail, D. Rana and T. Matsuura, *Chem. Eng. J.*, **198-199**, 327 (2012).
33. S. Srisurichan, R. Jiraratananon and A. G. Fane, *J. Membr. Sci.*, **277**, 186 (2006).
34. Gh. Bakeri, T. Matsuura and A. F. Ismail, *J. Membr. Sci.*, **383**, 159 (2011).
35. C. H. Loh and R. Wang, *Chin. J. Chem. Eng.*, **20**(1), 71 (2012).
36. Q. F. Alsalhy, H. A. Salih, S. Simone, M. Zablouk, E. Drioli and A. Figoli, *Desalination*, **345**, 21 (2014).
37. E. Fontananova, J. C. Jansen, A. Cristiano, E. Curcio and E. Drioli, *Desalination*, **192**, 190 (2006).
38. Gh. Bakeri, A. F. Ismail, M. Rezaei DashtArzhandi and T. Matsuura, *J. Membr. Sci.*, **475**, 57 (2015).
39. J. L. Li and B. H. Chen, *Sep. Purif. Technol.*, **41**, 109 (2005).